Solvatomorphic Phase Transitions and Tunable Luminescence Emission in Lanthanide Metal-Organic Frameworks

Alena A. Vasileva[1,2], Pavel A. Demakov[1], Tatiana Y. Guselnikova[1], Alexey A. Ryadun[1], Vladimir P. Fedin[1], Danil N. Dybtsev[1].

1 Nikolaev Institute of Inorganic Chemistry, Siberian Branch of the Russian Academy of Sciences, 630090 Novosibirsk, Russia

2 Department of Natural Sciences, Novosibirsk State University, 2 Pirogova St., 630090 Novosibirsk, Russia

Electronic supplementary information

Trans-1,4-cyclohexanedicarboxylic acid (H_2chdc, >97.0%) was received from BLD Pharmatech. 1,10-phenanthroline monohydrate (phen·H_2O, >98.0%) was received from Chimreagent (Ufa, Russia). N,N-dimethylformamide (DMF, reagent grade) and N,N-dimethylacetamide (DMA, >99.95%) were received from Vekton (Saint Petersburg, Russia). N,N-diethylformamide (DEF, 99%) was received from Sigma Aldrich. N-formylpiperidine (NFP, >98.0%) was received from TCI. Samarium(III) nitrate hexahydrate (high-purity grade) was received from Novosibirsk Rare Metals Plant. All reagents were used as received without further purification.

IR spectra in KBr pellets were recorded in the range 4000−400 cm^{-1} on a Bruker Scimitar FTS 2000 spectrometer (Billerica, MA, USA). Elemental analysis was conducted with a VarioMICROcube (Elementar Analysensysteme GmbH, Hanau, Germany) analyzer. Powder X-ray diffraction (PXRD) analysis was performed at room temperature on a Bruker D8 Advance (Billerica, MA, USA) diffractometer (Cu-Kα radiation, λ = 1.54178 Å). Thermogravimetric analysis was carried out using a Netzsch TG 209 F1 Iris (Selb, Germany) instrument under Ar flow (30 $cm^3 \cdot min^{-1}$) at a 10 $K \cdot min^{-1}$ heating rate. Photoluminescence excitation and emission spectra and excited state lifetimes were recorded with a spectrofluorometer Horiba Jobin Yvon Fluorolog 3 equipped with ozone-free Xe-lamp 450W power, cooled photon detector R928/1860 PFR technologies with refrigerated chamber PC177CE-010 and double-grating monochromators. The spectra were corrected for source intensity and detector spectral response by standard correction curves. Solution UV absorption spectra were recorded on OKB Spectr SF-2000 spectrophotometer. Inductively coupled plasma atomic emission spectrometry (ICP AES) (or optical emission spectrometry ICP OES) was used to quantify samarium and terbium in samples. ICP AES measurements were carried out using Grand-ICP spectrometer (VMK Optoelektronika, Novosibirsk, Russia) with axial view of the plasma, pneumatic nebulizer OneNeb (Agilent Technologies, Santa Clara, USA) cyclonic spray chamber (Precision Glassblowing, Centennial, USA). The spectral range of the ICP spectrometer is from 190 to 780 nm. The following argon flows were used for quantitative measurements: plasma gas flow 12 L min^{-1}, auxiliary gas flow 0.40 L min^{-1}, nebulizer flow 0.45 L min^{-1}. Power supplied to an ICP inductor was 1300 W. The samples were digested in a mixture of HCl 36% water solution and H_2O_2 30% water solution, then diluted by 0.5 mol L^{-1} HNO_3 prior to ICP-AES analysis. Calibration curves were obtained using commercial multielement standard solutions MES (Skat, Novosibirsk, Russia). Multielement standard solution MES (Skat, Novosibirsk, Russia) was used to determine the content of samarium and terbium. Diffraction data for single crystals of **1**–**4** were collected with an automated Agilent Xcalibur diffractometer equipped with an AtlasS2 area detector and graphite monochromator

($\lambda(MoK_\alpha) = 0.71073$ Å). The CrysAlisPro[1] program package was used for the integration, absorption correction and determination of unit cell parameters. The dual space algorithm (SHELXT[2]) was used for the structure solution and the full-matrix least-squares technique (SHELXL[3]) was used for structure refinement. Anisotropic approximation was applied for all atoms, except hydrogens. Positions of hydrogen atoms were calculated geometrically and refined in the riding model. For **4**, a non-merohedral twinning with an orientation matrix (–0.9997 0.0002 –0.0009 –0.1401 1.0000 –0.0046 0.0024 0.0018 –1.0001) and second component weight (BASF) of 0.3911 was found and accounted using CrysAlisPro software during initial frame processing and integration. The BASF value 0.31716 reported in cif file was obtained after the complete crystal structure refinement. Details for single-crystal structure determination experiments and structure refinements are summarized in Table S1. CCDC 2381788–2381791 entries contain the supplementary crystallographic data for this paper. These data can be obtained free of charge from The Cambridge Crystallographic Data Center at https://www.ccdc.cam.ac.uk/structures/.

Table S1. Single-crystal X-ray diffraction experiment and structure refinement details

1	**1**	**2**	**3**	**4**
Chemical formula	$C_{46}H_{50}N_8O_{16}Sm_2$	$C_{48}H_{54}N_8O_{16}Sm_2$	$C_{50}H_{58}N_8O_{16}Sm_2$	$C_{52}H_{58}N_8O_{16}Sm_2$
M_r, g·mol^{-1}	1271.64	1299.69	1327.74	1351.76
Crystal system	Triclinic	Monoclinic	Monoclinic	Triclinic
Space group	$P\bar{1}$	$P2_1/n$	$P2_1/c$	$P\bar{1}$
Temperature, K	293	290	291	292
a, Å	10.3761(3)	12.6382(5)	12.9332(4)	13.0555(7)
b, Å	10.7077(3)	16.9640(5)	13.7559(3)	13.9456(7)
c, Å	12.8832(4)	12.8442(5)	16.2253(5)	15.9707(7)
α, °	68.299(3)	90	90	88.323(4)
b, °	68.228(2)	113.567(5)	111.620(4)	68.432(4)
γ, °	81.243(2)	90	90	86.135(4)
V, Å^3	1234.87(7)	2524.04(18)	2683.53(15)	2698.0(2)
Z	1	2	2	2
F(000)	634	1300	1332	1356
$D_{(calc.)}$, g·cm^{-3}	1.710	1.710	1.643	1.664
μ, mm^{-1}	2.43	2.38	2.24	2.23
Crystal size, mm	0.32 × 0.11 × 0.10	0.20 × 0.09 × 0.08	0.46 × 0.10 × 0.10	0.34 × 0.09 × 0.07
θ range for data collection, °	2.05 < θ < 25.35	2.11 < θ < 25.35	2.25 < θ < 25.35	2.00 < θ < 25.35
No. of reflections: measured / independent / obs. [I > 2σ(I)]	9099 / 4520 / 4223	11894 / 4633 / 3977	21148 / 4918 / 4473	9661 / 9661 / 7851
R_{int}	0.0233	0.0223	0.0649	–
Index ranges	$-12 \le h \le 10$ $-12 \le k \le 12$ $-15 \le l \le 15$	$-13 \le h \le 15$ $-20 \le k \le 20$ $-12 \le l \le 15$	$-15 \le h \le 15$ $-16 \le k \le 16$ $-19 \le l \le 19$	$-14 \le h \le 15$ $-16 \le k \le 16$ $-19 \le l \le 19$
Final R indices [I > 2σ(I)]	$R_1 = 0.0233$ $wR_2 = 0.0540$	$R_1 = 0.0215$ $wR_2 = 0.0431$	$R_1 = 0.0284$ $wR_2 = 0.0743$	$R_1 = 0.0603$ $wR_2 = 0.1641$
Final R indices (all data)	$R_1 = 0.0262$ $wR_2 = 0.0552$	$R_1 = 0.0298$ $wR_2 = 0.0453$	$R_1 = 0.0316$ $wR_2 = 0.0775$	$R_1 = 0.0750$ $wR_2 = 0.1735$
Goodness-of-fit on F^2	1.051	1.047	1.071	1.053
Largest diff. peak, hole, e/Å^3	0.61, –0.63	0.35, –0.41	0.67, –0.66	2.40, –1.71

Table S2. Bond lengths in Sm^{3+} coordination environment in **1**–**4**.

		Structure				
Part of the capped square antiprism	Atom type	**1**	**2**	**3**	**4** (Sm1)	**4** (Sm2)
Base square	N(phen)	2.591(3); 2.638(3)	2.599(2); 2.635(2)	2.593(3); 2.634(2)	2.606(8); 2.649(8)	2.594(8); 2.646(8)
	O(κ^2-NO_3)	2.504(3); 2.546(3)	2.498(2); 2.5664(19)	2.536(2); 2.545(2)	2.471(8); 2.563(7)	2.498(8); 2.574(7)
Upper square	O(μ-κ^1:κ^1-COO)	2.353(2); 2.367(2)	2.3537(17); 2.3615(18)	2.348(2); 2.3480(19)	2.363(6); 2.371(7)	2.338(6); 2.367(6)
	O(μ-κ^1:κ^2-COO)	2.3650(19); 2.482(2)	2.3623(17); 2.4626(17)	2.363(2); 2.409(2)	2.359(6); 2.454(6)	2.338(7); 2.429(7)
Cap		2.570(2)	2.6106(18)	2.749(2)	2.585(6)	2.762(6)

Table S3. Compositions of mixed-metal samples.

Sample	Sm : Tb ratio		Final formula $[Ln_2(phen)_2(NO_3)_2(chdc)_2]\cdot 2solv$, Ln_2 =
	Theoretical	Determined by ICP-AES	
1$_{Tb}$	97 : 0 : 3	96.6 : 0 : 3.4	$Sm_{1.932}Tb_{0.068}$
2$_{Tb}$	95 : 0 : 5	98.2 : 0 : 1.8	$Sm_{1.964}Tb_{0.036}$
3$_{Tb}$	95 : 0 : 5	91.7 : 0 : 8.3	$Sm_{1.834}Tb_{0.166}$
4$_{Tb}$	95 : 0 : 5	91.2 : 0 : 8.8	$Sm_{1.824}Tb_{0.176}$

Table S4. Main solvent characteristics.

Name	Abbre-viation	Chemical formula	Dielectric constant, F/m	Molecular size, Å	Boiling temperature, °C
N,N-Dimethylformamide	DMF	C_3H_7NO	36.1	4 x 6 x 6	153
N,N-Dimethylacetamide	DMA	C_4H_9NO	38.1	4 x 7 x 7	165.5
N,N-diethylformamide	DEF	$C_5H_{11}NO$	28.4	5 x 7 x 8	178.3
N-Formylpiperidine	NFP	$C_6H_{11}NO$	26.2	5 x 6.5 x 8	222

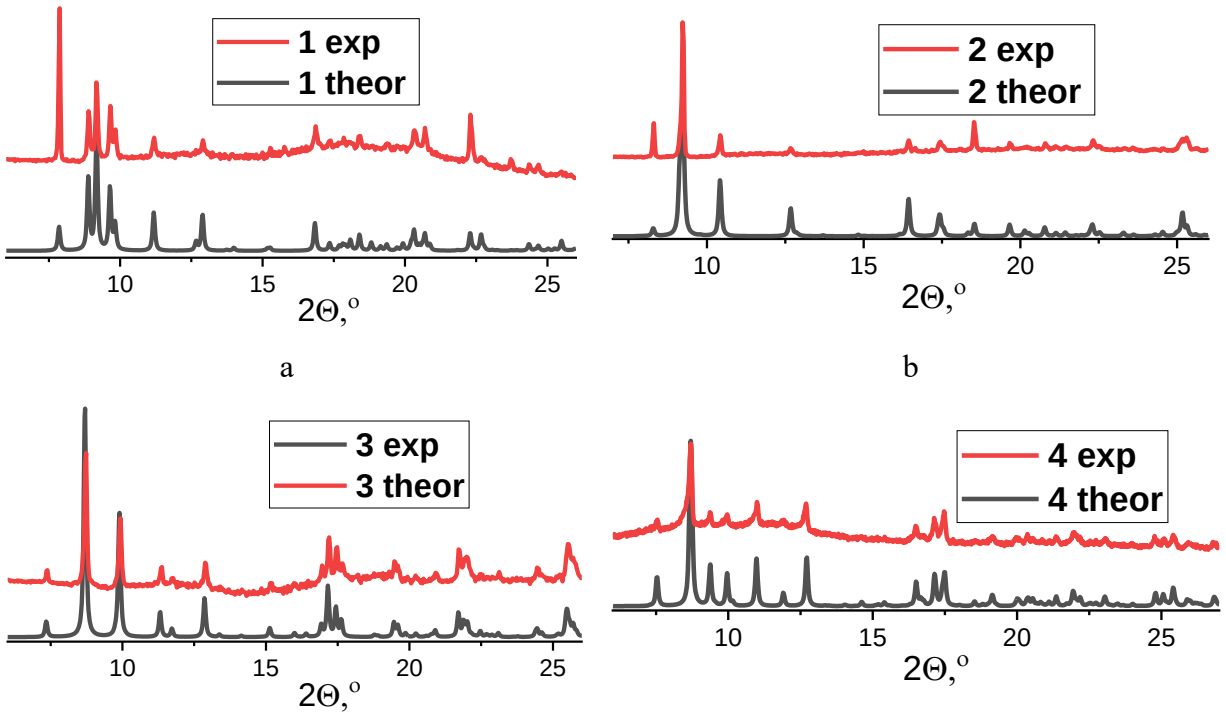

Fig. S1. PXRD patterns for compounds **1** (a), **2** (b), **3** (c) and **4** (d) compared to the theoretical ones.

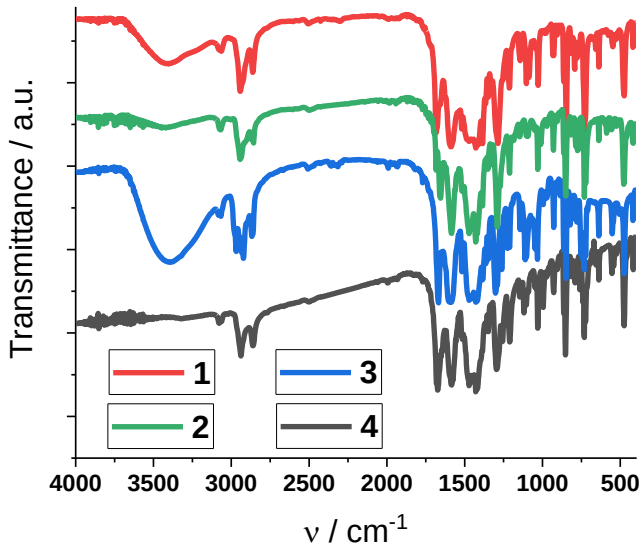

Fig. S2. IR spectra for compounds **1**–**4**.

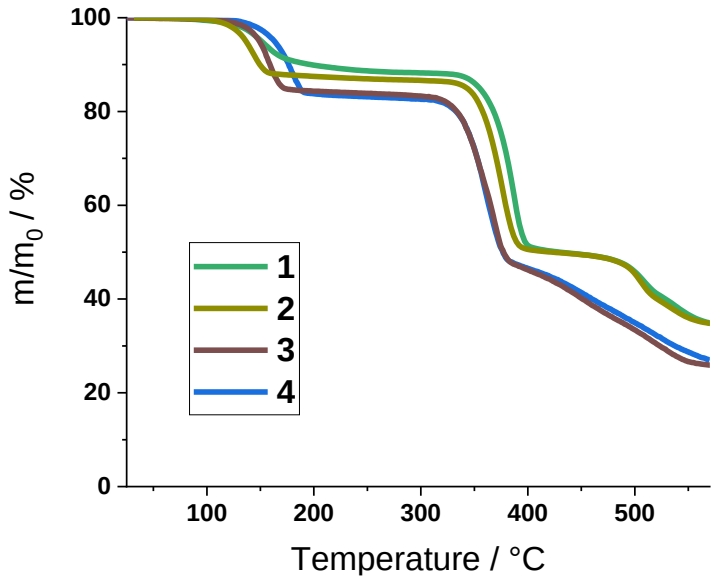

Fig. S3. TG plots for compounds **1**–**4**.

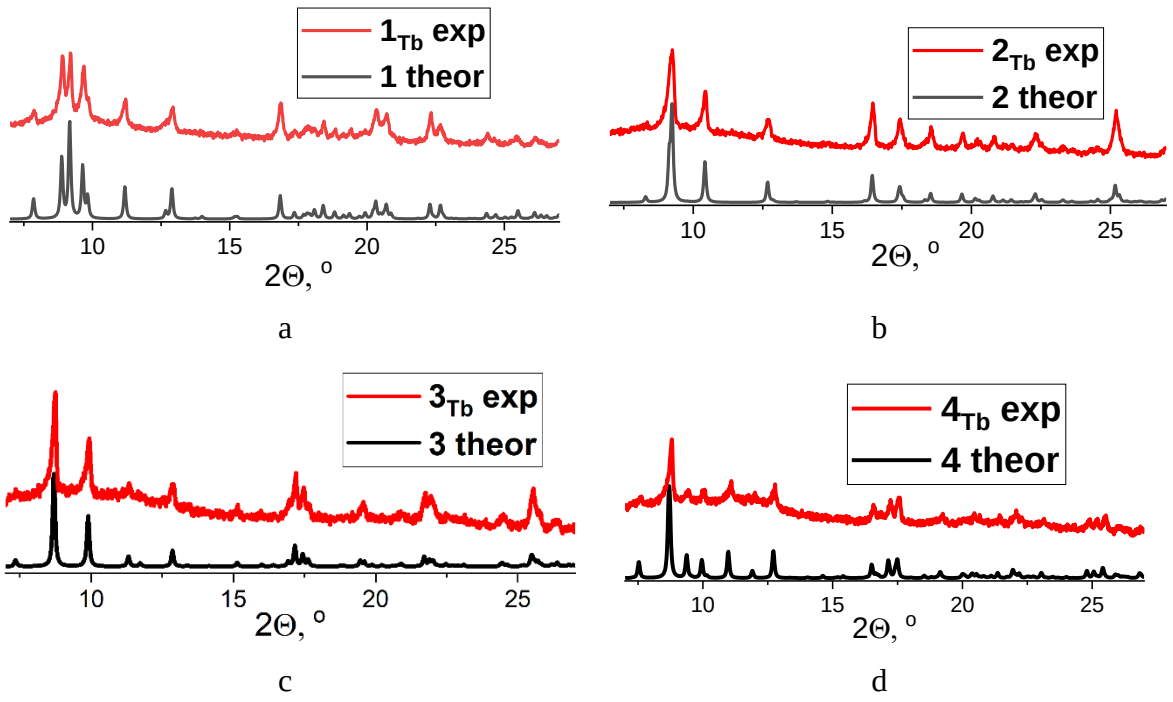

Fig. S4. PXRD patterns for the samples **1**$_{Tb}$ (a), **2**$_{Tb}$ (b), **3**$_{Tb}$ (c) and **4**$_{Tb}$ (d), compared to the theoretical patterns for **1**–**4**.

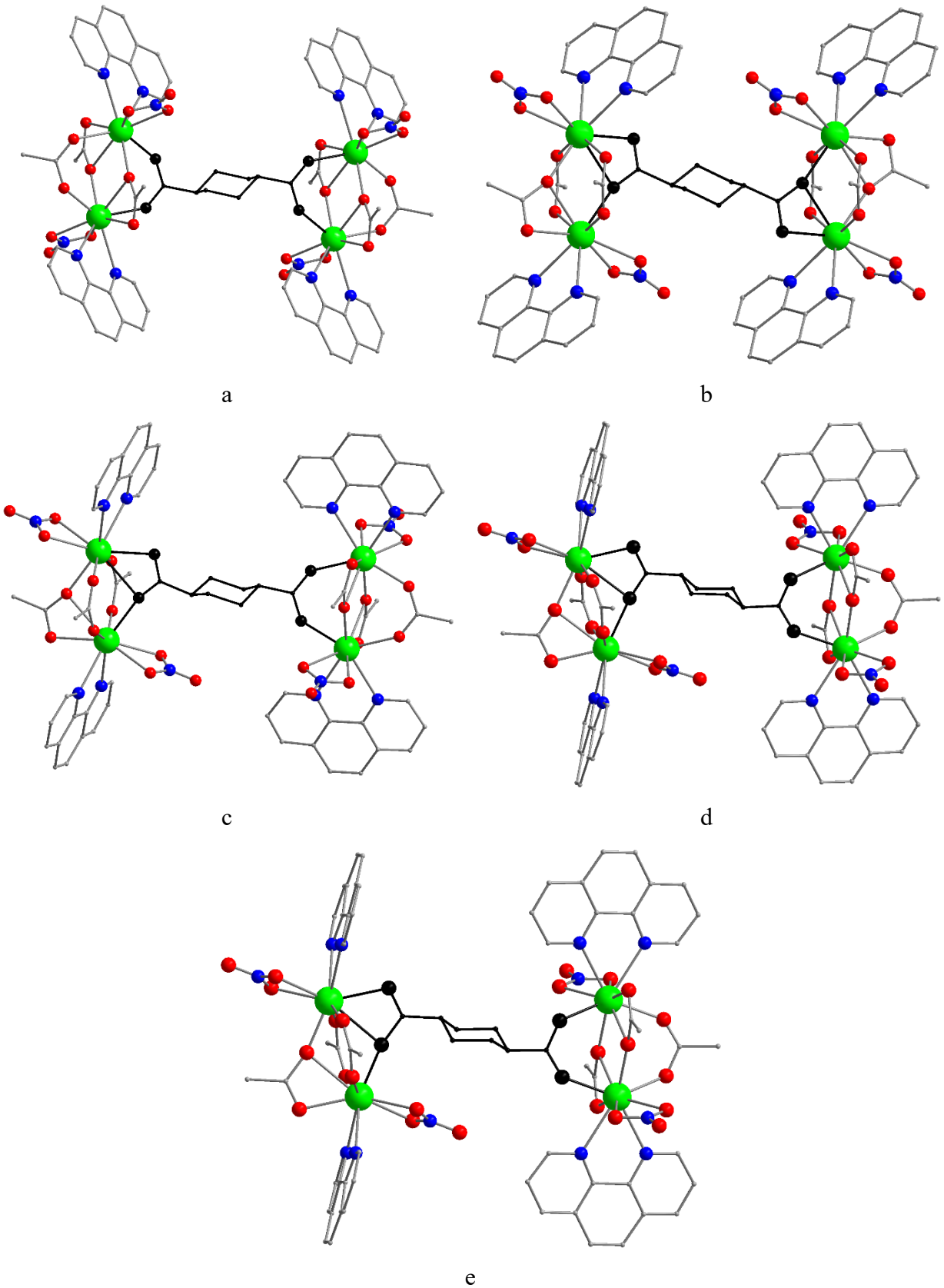

Fig. S5. Coordination modes of $chdc^{2-}$ ligand in **1** (a,b), **2** (c), **3** (d) and **4** (e).

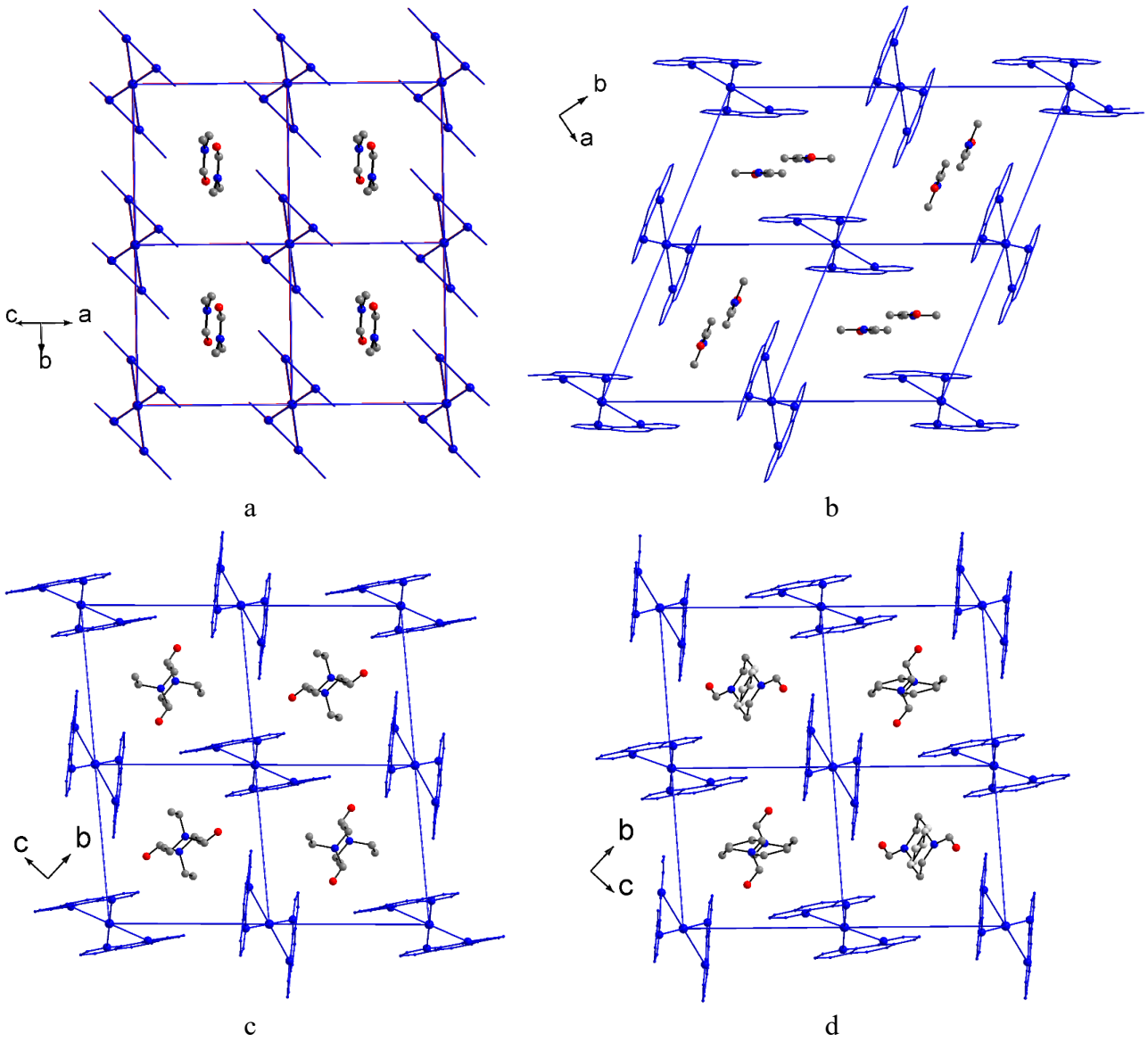

Fig. S6. Packing of the guest solvent molecules in **1** (a), **2** (b), **3** (c) and **4** (d). C atoms are grey, O atoms are red. H atoms are not shown. Binuclear metal blocks and chdc bridges are shown as nodes and edges, respectively.

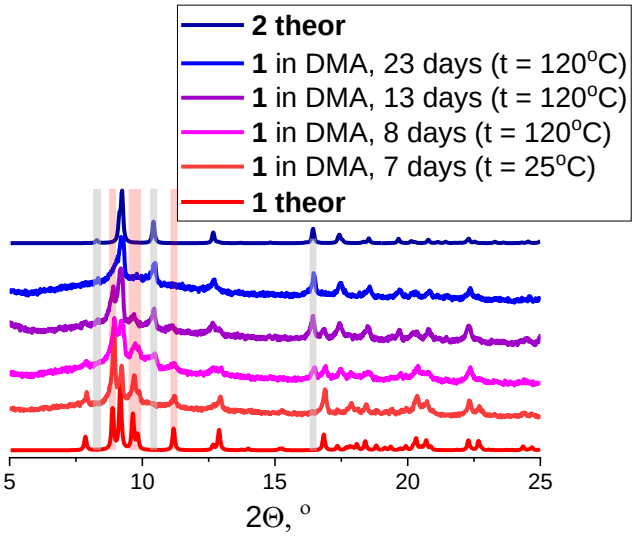

a

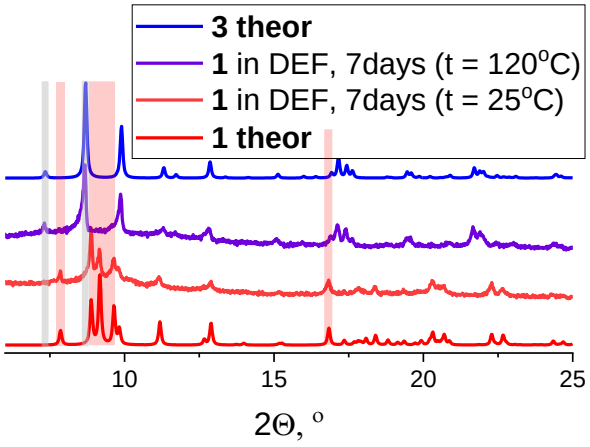

b

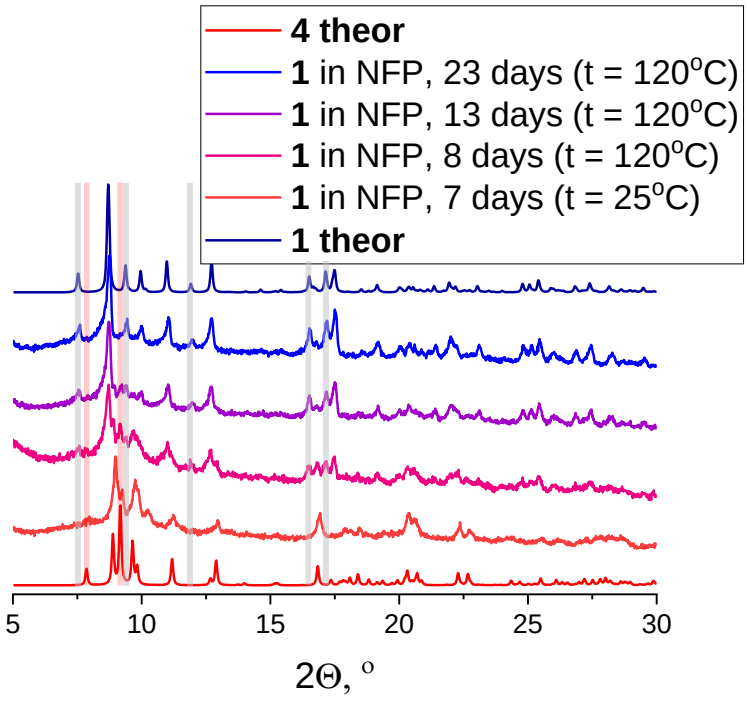

c

Fig. S7. PXRD patterns for the **1**→**2** (a), **1**→**3** (b) and **1**→**4** (c) phase transitions.

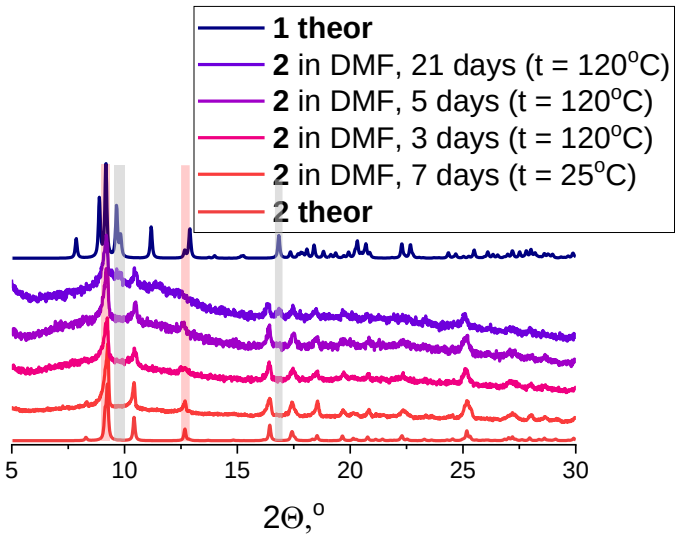

a

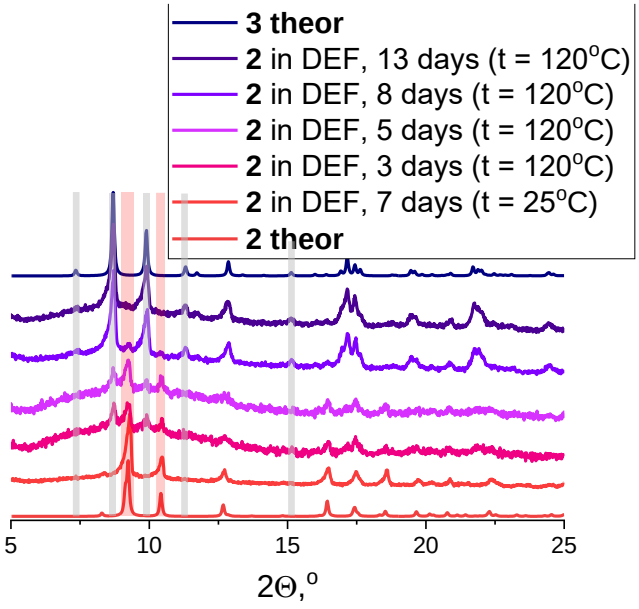

b

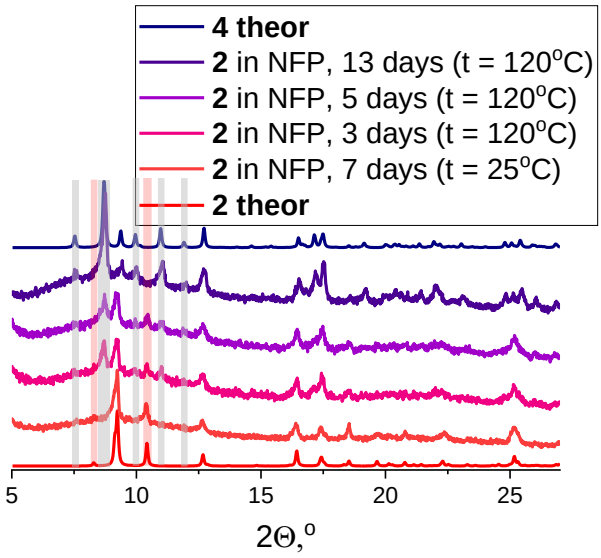

c

Fig. S8. PXRD patterns for the **2**→**1** (a), **2**→**3** (b) and **2**→**4** (c) phase transitions.

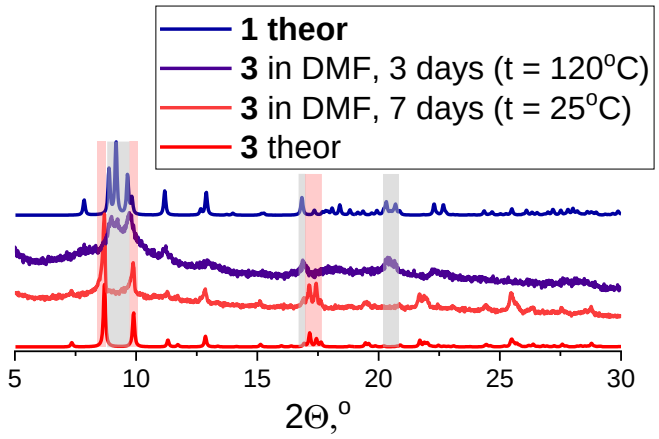

a

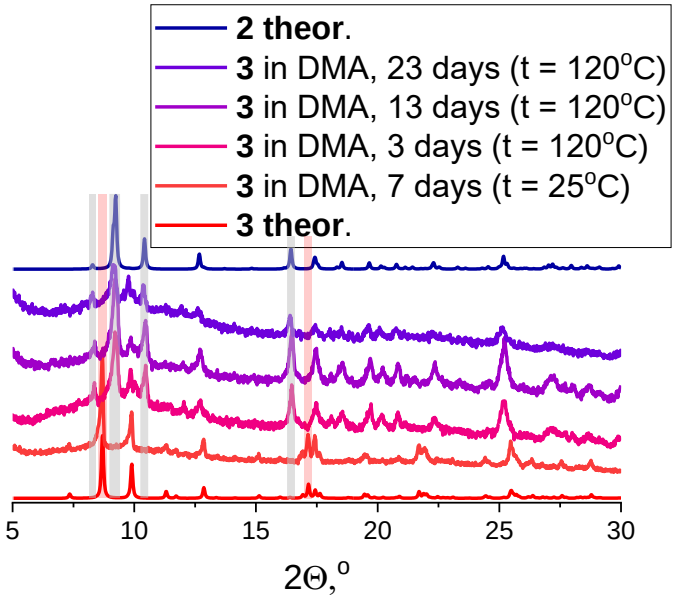

b

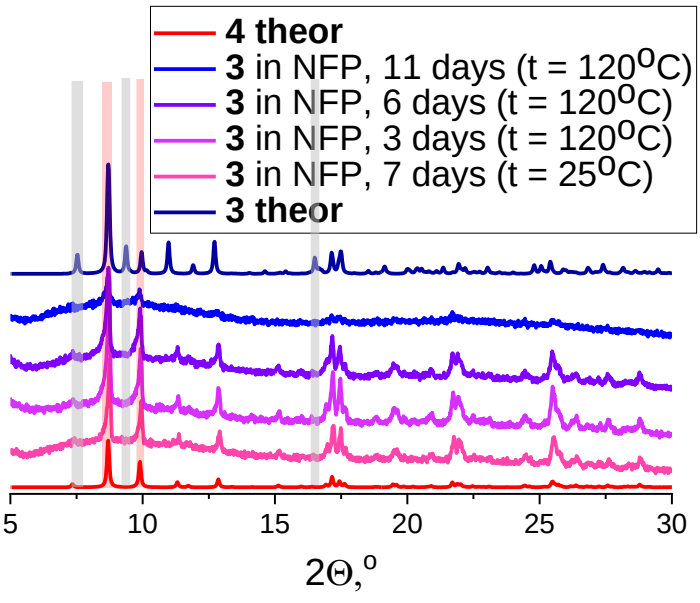

c

Fig. S9. PXRD patterns for the **3**→**1** (a), **3**→**2** (b) and **3**→**4** (c) phase transitions.

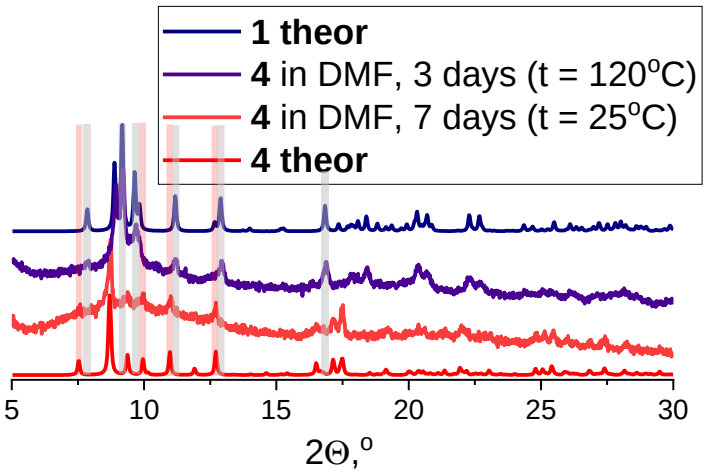

a

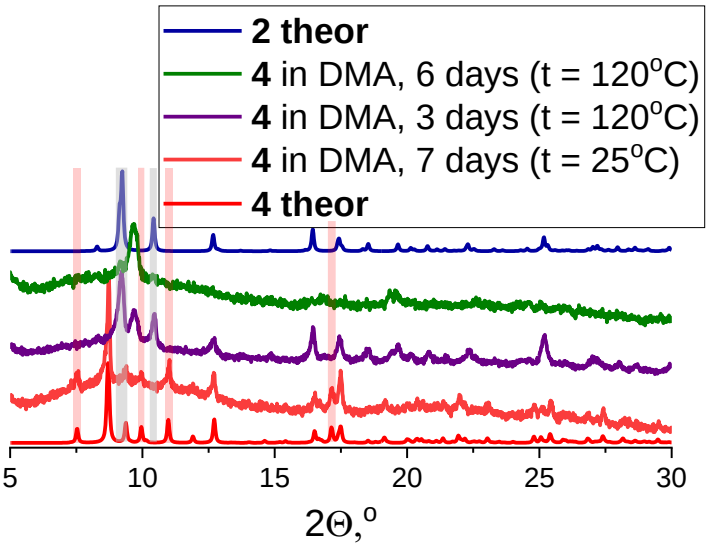

b

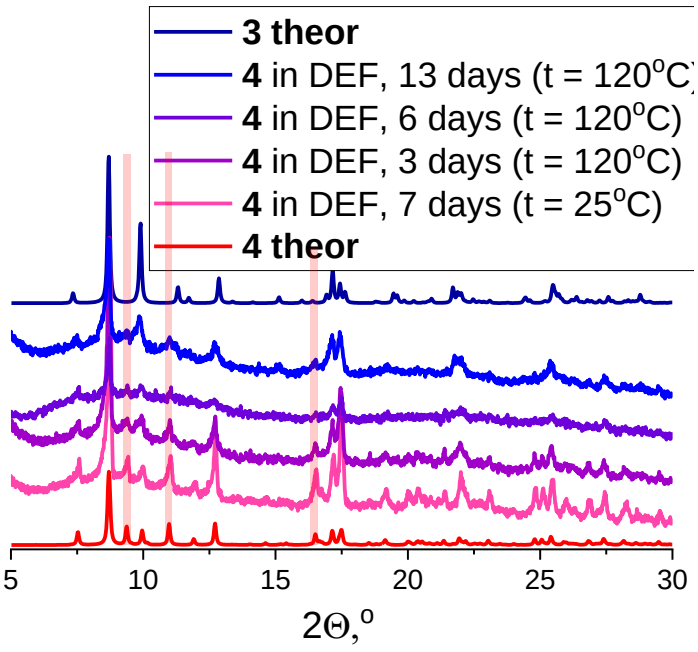

c

Fig. S10. PXRD patterns for the **4→1** (a), **4→2** (b) and **4→3** (c) phase transitions.

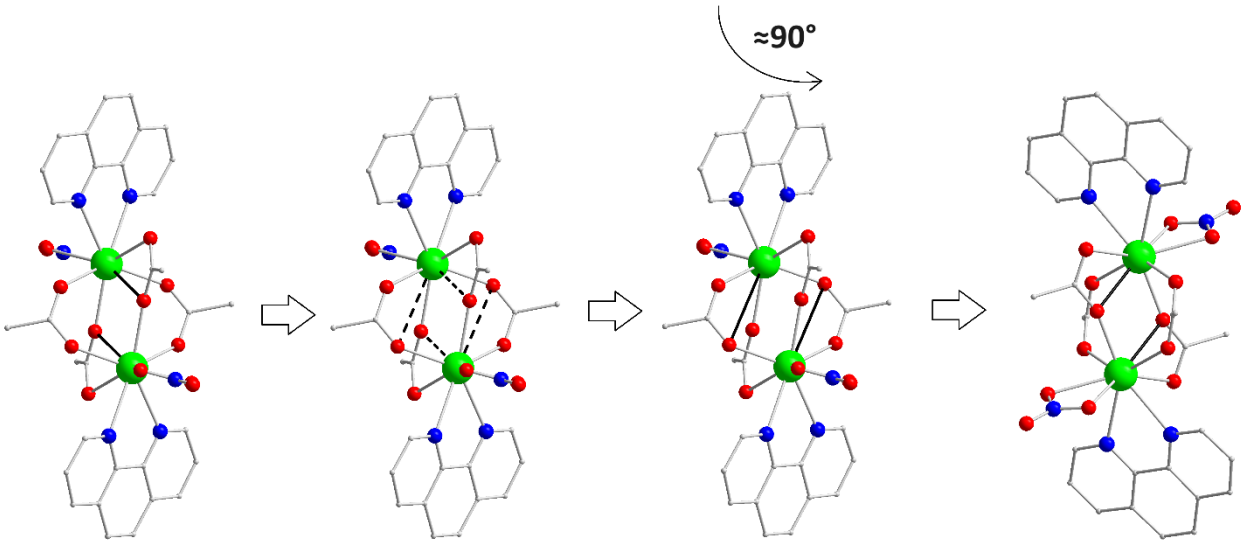

Fig. S11. A schematical illustration of possible mechanism of Sm-phen-carboxylate block rearrangement. Black lines show rearranging bonds, providing a rotation of the overall block.

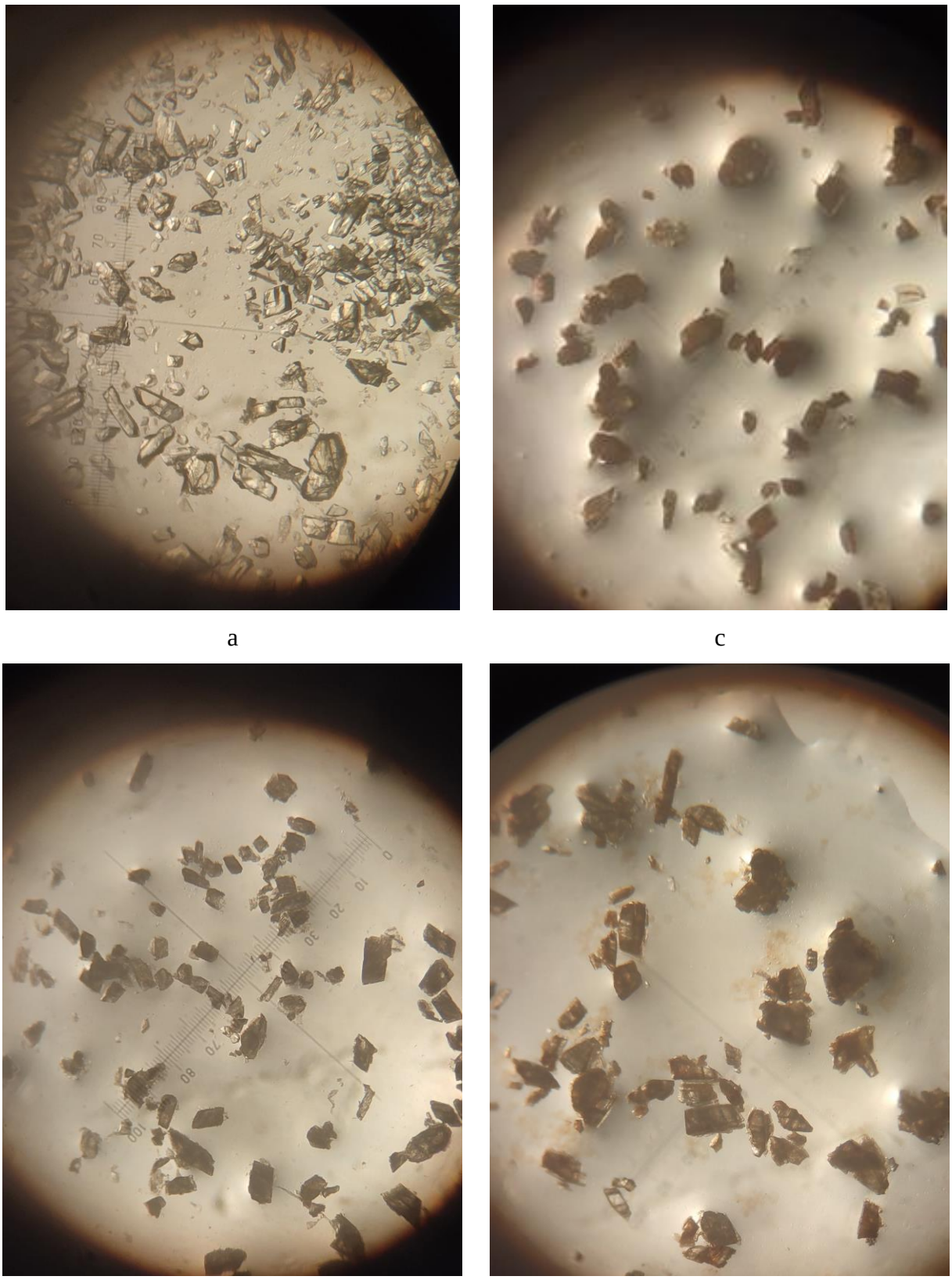

Fig. S12. Photographs of sample **1**: as-synthesized (a), after immersion for 3 days in DMA (b), after immersion for 3 days in DEF (c) and after immersion for 3 days in NFP (d).

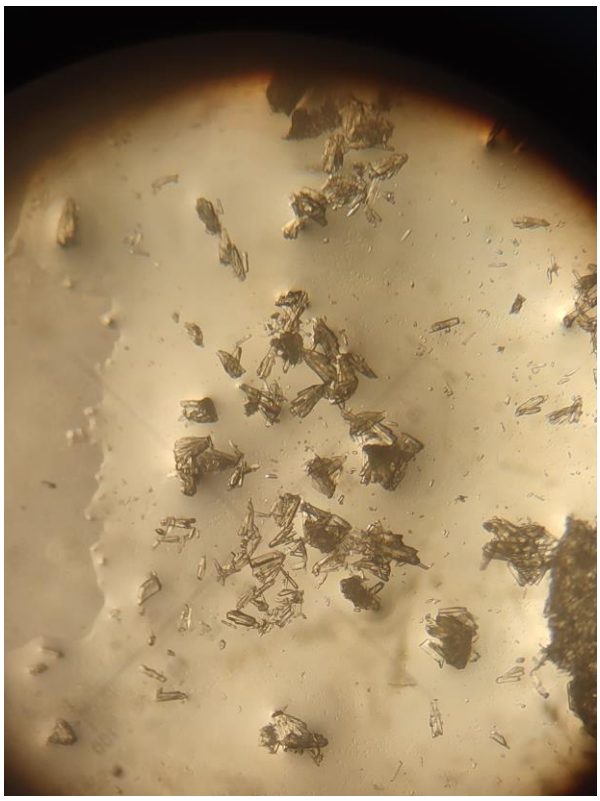

a

c

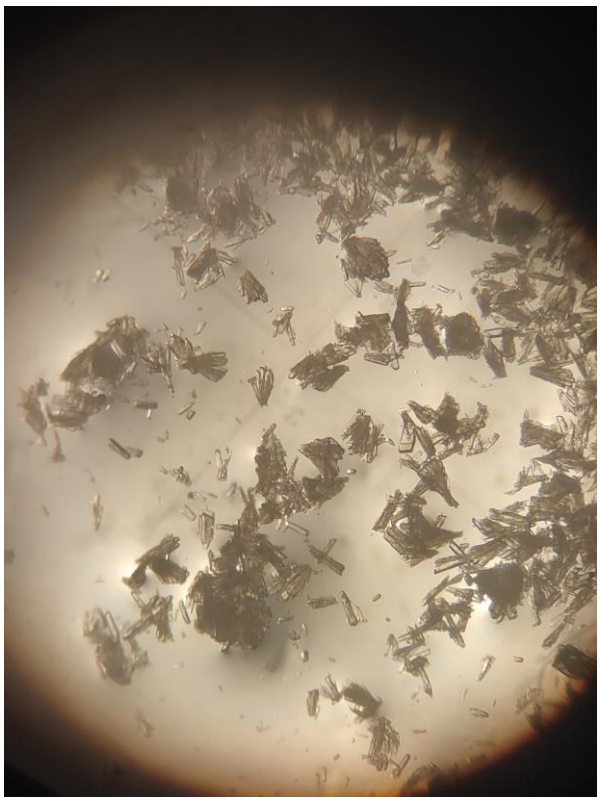

b

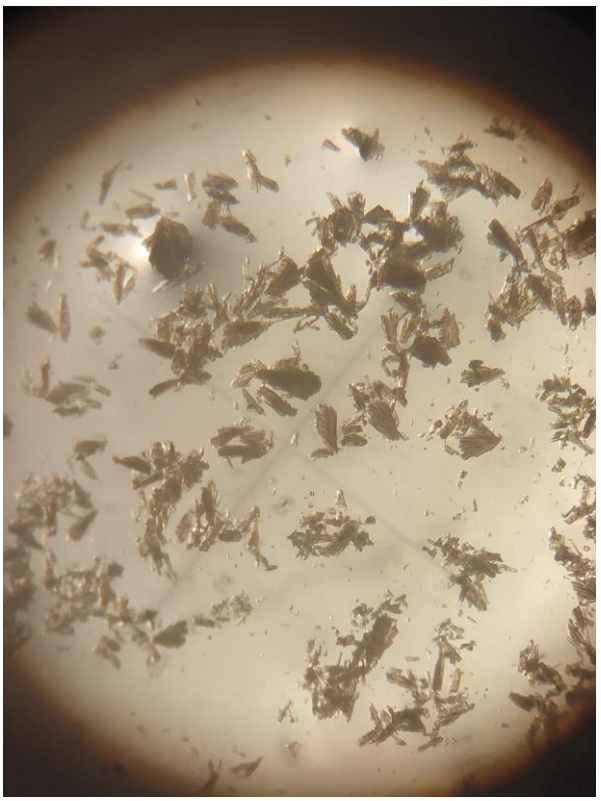

d

Fig. S13. Photographs of sample **2**: as-synthesized (a), after immersion for 3 days in DMF (b), after immersion for 3 days in DEF (c) and after immersion for 3 days in NFP (d).

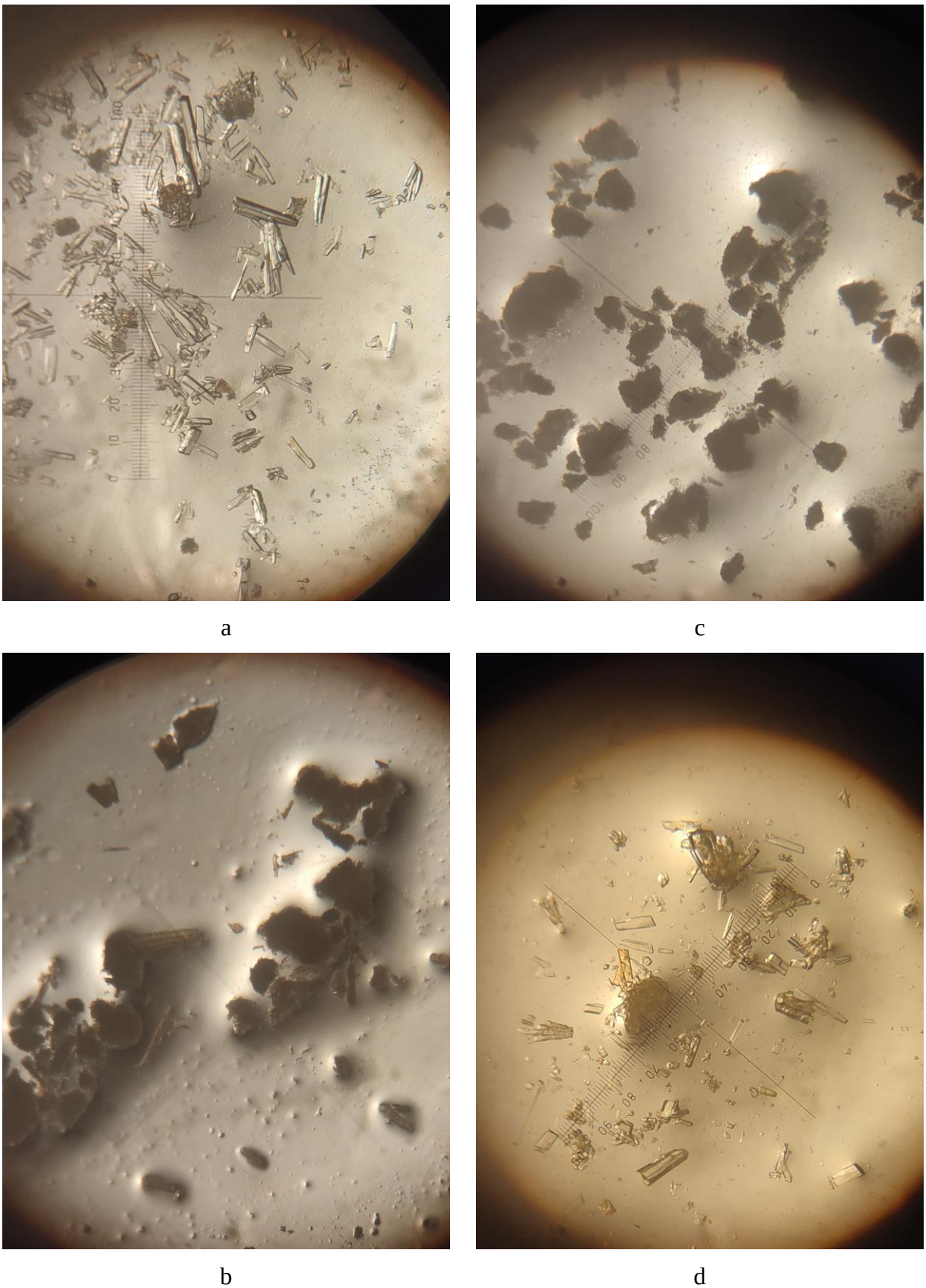

a c

b d

Fig. S14. Photographs of sample **3**: as-synthesized (a), after immersion for 3 days in DMF (b), after immersion for 3 days in DMA (c) and after immersion for 3 days in NFP (d).

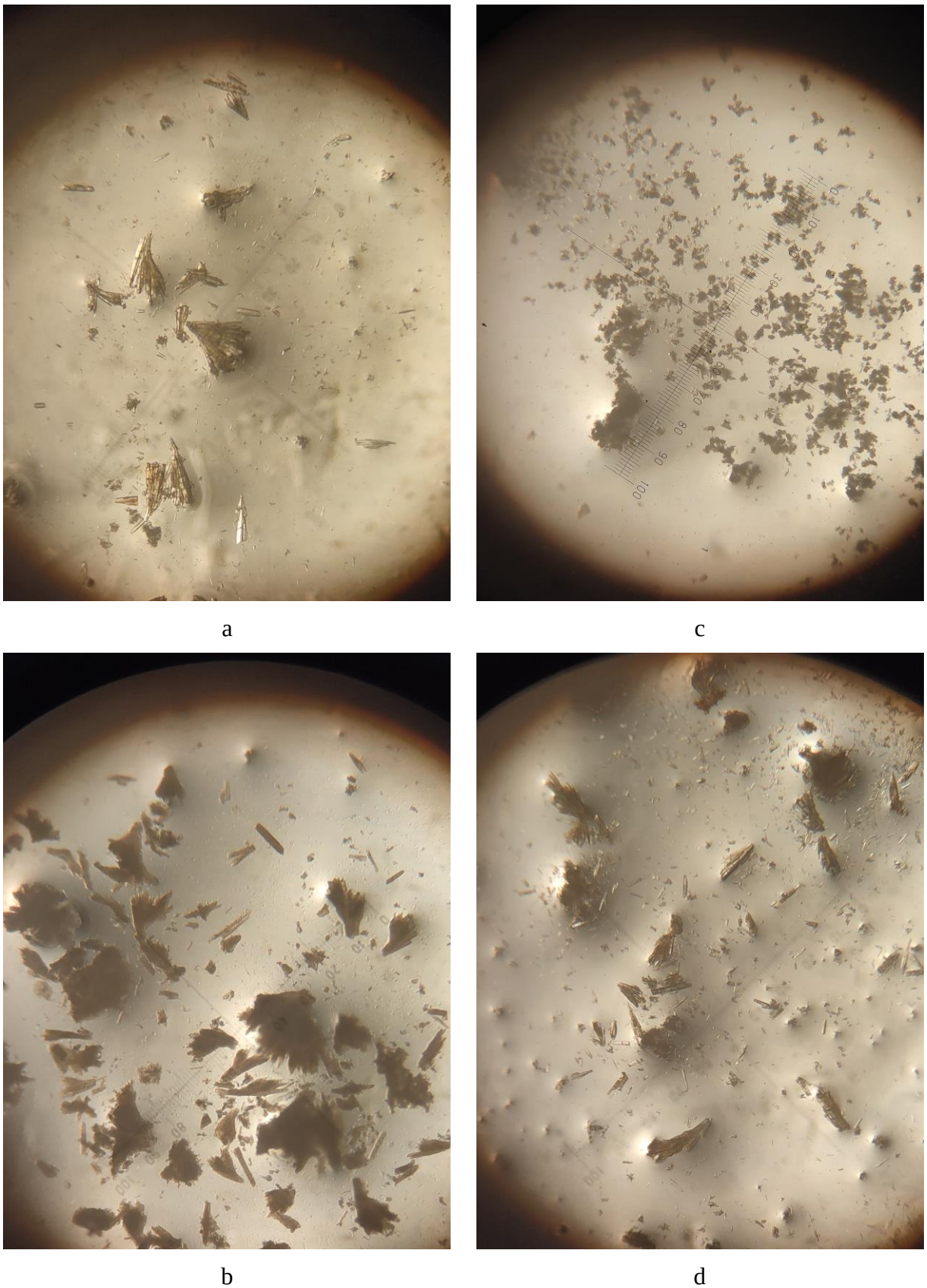

Fig. S15. Photographs of sample **4**: as-synthesized (a), after immersion for 3 days in DMF (b), after immersion for 3 days in DMA (c) and after immersion for 3 days in DEF (d).

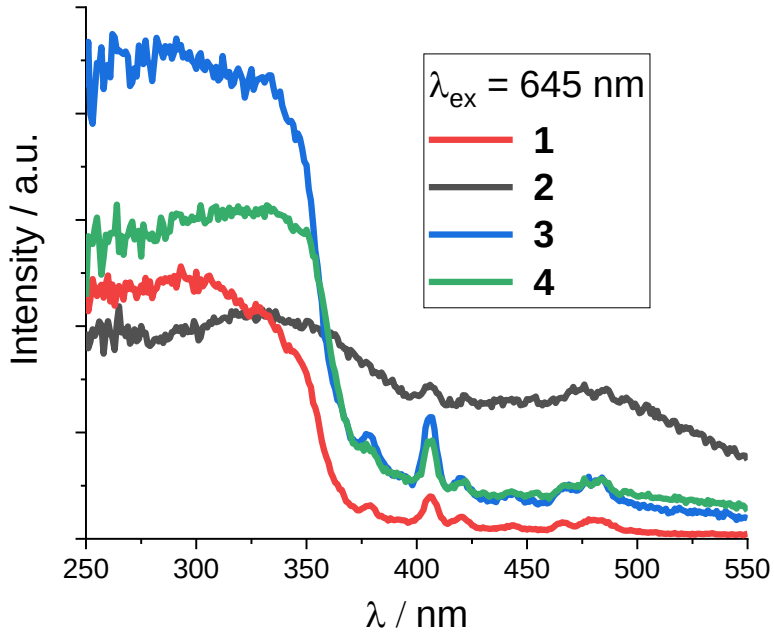

Fig. S16. Excitation spectra for compounds **1**–**4**.

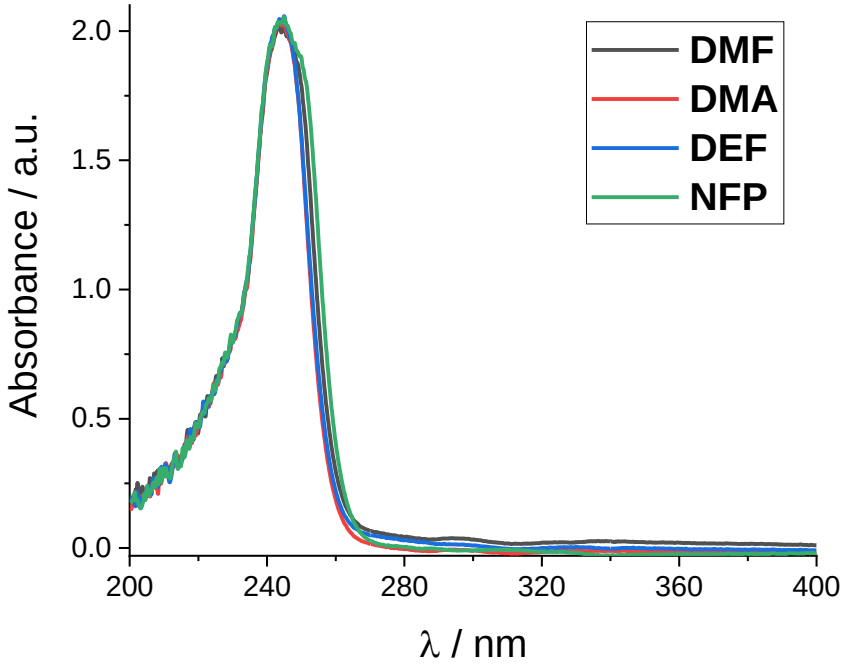

Fig. S17. UV absorption spectra of the used solvents (1.0% v/v in THF), normalized of the intensity maximum.

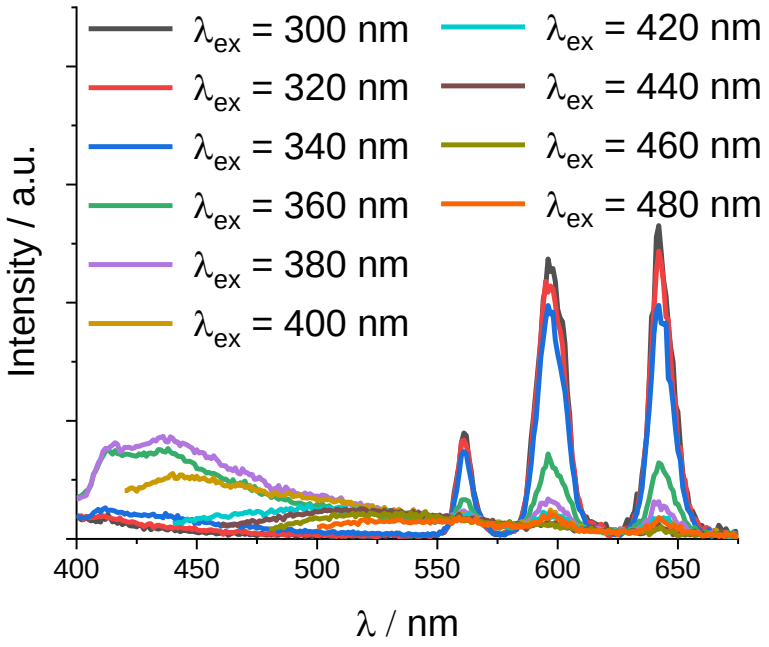

Fig. S18. Emission spectra for $\mathbf{1_{Tb}}$ upon varying excitation wavelength.

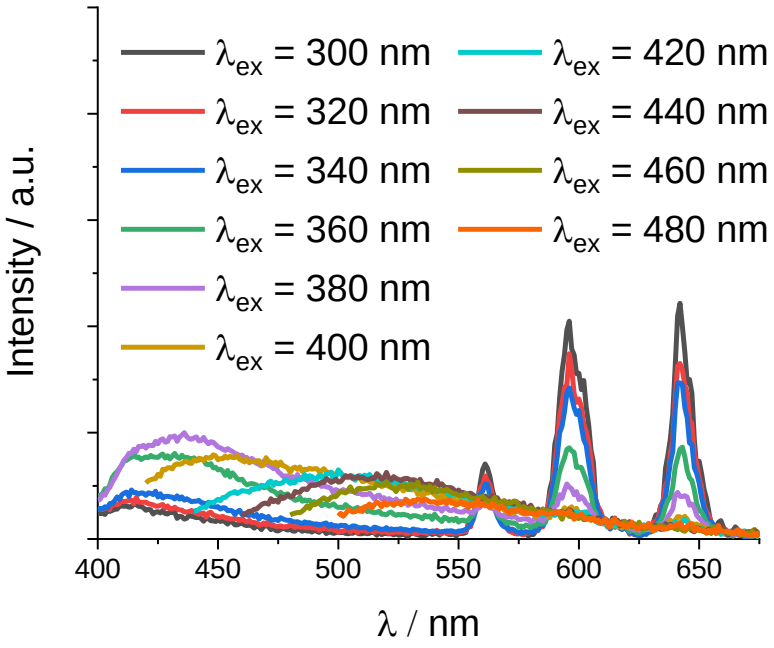

Fig. S19. Emission spectra for $\mathbf{2_{Tb}}$ upon varying excitation wavelength.

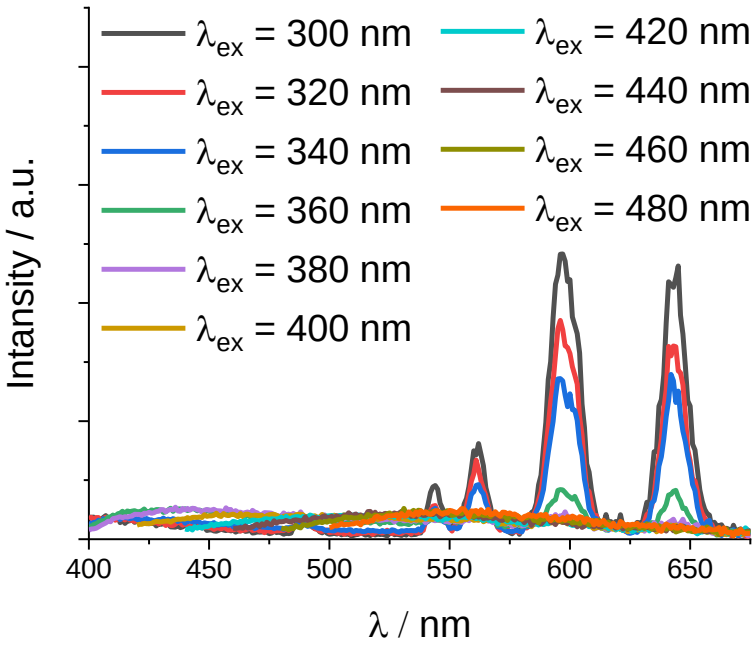

Fig. S20. Emission spectra for **3**$_{Tb}$ upon varying excitation wavelength.

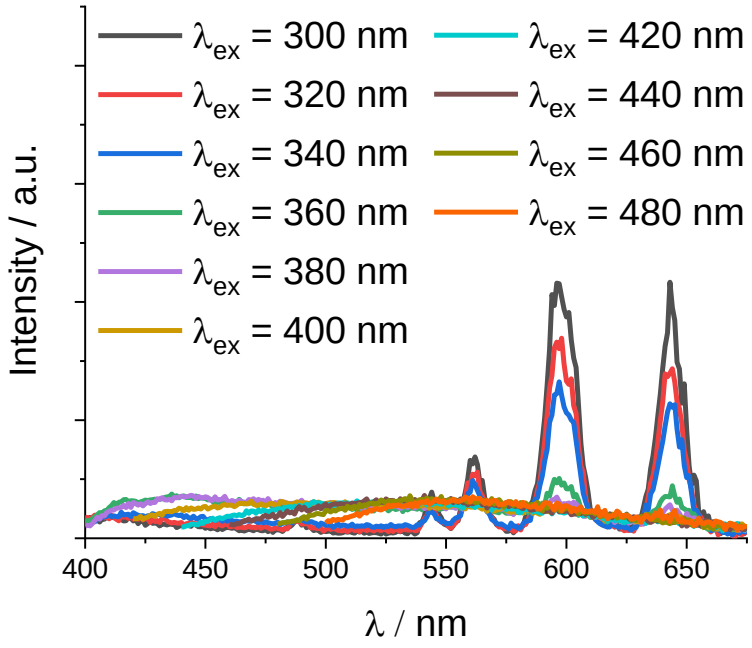

Fig. S21. Emission spectra for **4**$_{Tb}$ upon varying excitation wavelength.

Fig. S22. Digital photographs of the Tb-doped samples. From left to right: λ_{ex} = 340 nm, 360 nm, 380 m, 400 nm. From top to down: samples **1**$_{Tb}$, **2**$_{Tb}$, **3**$_{Tb}$, **4**$_{Tb}$.

Table S5. Experimental excited state lifetimes for the samples.

Sample	τ_l, μs (λ_{ex} = 380 nm, λ_{em} = 595 nm)	Sample	τ_l, μs (λ_{ex} = 380 nm, λ_{em} = 595 nm)
1	39(2)	**1**$_{Tb}$	54.6(14)
2	46(2)	**2**$_{Tb}$	44.9(14)
3	48(3)	**3**$_{Tb}$	55(3)
4	43(2)	**4**$_{Tb}$	43.2(19)

References

1. CrysAlisPro 1.171.38.46. Rigaku Oxford Diffraction: The Woodlands, TX, USA, 2015.
2. G.M. Sheldrick, *Acta Crystallogr.*, 2015, **A71**, 3-8. https://doi.org/10.1107/S2053273314026370
3. G.M. Sheldrick, *Acta Crystallogr.*, 2015, **C71**, 3-8. https://doi.org/10.1107/S2053229614024218